Title
Phase Behavior of Mixtures of Block Copolymers and a Lithium Salt

Journal
The Journal of Physical Chemistry B, 122(33)

ISSN
1520-6106

Authors
Loo, Whitney S
Galluzzo, Michael D
Li, Xiuhong
et al.

Publication Date
2018-08-23

DOI
10.1021/acs.jpcb.8b04189

Peer reviewed

Phase Behavior of Mixtures of Block Copolymers and a Lithium Salt

Whitney S. Loo [†], Michael D. Galluzzo [†, a], Xiuhong Li [‡], Jacqueline A. Maslyn [†, a], Hee Jeung Oh [†], Katrina I. Mongcopa [†], Chenhui Zhu [b], Andrew A. Wang [†], Xin Wang [‡], Bruce A. Garetz [‡], Nitash P. Balsara [*, †, ‡,]

[†] Department of Chemical and Biomolecular Engineering, University of California-Berkeley, Berkeley, California 94720, United States

‡ Department of Chemical and Biomolecular Engineering, NYU Tandon School of Engineering, Brooklyn, NY 11201, United States

[a] Materials Sciences Division, Lawrence Berkeley National Laboratory, Berkeley California 94720, United States

[b] Advanced Light Source, Lawrence Berkeley National Laboratory, Berkeley California 94720, United States

 Energy Technologies Area, Lawrence Berkeley National Laboratory, Berkeley California 94720, United States

Abstract:

We present experimental results on the phase behavior of block copolymer/salt mixtures over a wide range of copolymer compositions, molecular weights and salt concentrations. The experimental system comprises polystyrene- *block* -poly(ethylene oxide) and lithium bis(trifluoromethanesulfonyl) imide (LiTFSI) salt. It is well established that LiTFSI interacts favorably with poly(ethylene oxide) relative to polystyrene. The relationship between chain length and copolymer composition at fixed temperature is U-shaped, as seen in experiments on conventional block copolymers and as anticipated from the standard self-consistent field theory (SCFT) of block copolymer melts. The phase behavior can be explained in terms of an effective Flory-Huggins interaction parameter between the polystyrene monomers and poly(ethylene oxide) monomers complexed with the salt, χ_{eff}, which increases linearly with salt concentration. The phase behavior of salt-containing block copolymers, plotted on a segregation strength versus copolymer composition plot, is similar to that of conventional (uncharged) block copolymer melts, when χ_{eff} replaces χ in segregation strength.

Introduction:

There is considerable interest in the potential use of microphase-separated block copolymers as solid electrolytes for lithium batteries.[1–4] Of particular interest are diblock copolymers that possess the ability to preferentially segregate salt into one of the microdomains. These microdomains provide channels for ion transport while other macroscopic properties, such as shear modulus, can be controlled by the nature of the other microdomain. A commonly studied system is polystyrene-*block*-poly(ethylene oxide) (SEO) mixed with lithium bis(trifluoromethanesulfonyl) imide salt, SEO/LiTFSI. The transport of lithium ions in poly(ethylene oxide) (PEO) has been fully characterized[5], and polystyrene (PS) acts as the mechanical support for the solid electrolyte.

The phase behavior of pure diblock copolymers has been thoroughly investigated.[6,7] The equilibrium phase behavior is controlled by two parameters: the volume fraction of one polymer block, f_A, and the segregation strength, χN, where N is the overall degree of polymerization and χ is the Flory-Huggins interaction parameter, which measures the thermodynamic compatibility between the two blocks. At high temperatures, entropic contributions dominate and the system forms a homogeneous disordered phase. As temperature decreases, interactions between the two polymer blocks become more important, which leads to microphase separation into ordered morphologies. For a given block copolymer, characterized by f_A and N, the transition from disorder-to-order occurs at a

critical value of χ, a parameter that generally increases as temperature decreases. The morphologies found in neat block copolymers include lamellae (LAM), bicontinuous gyroid phases (GYR), hexagonally packed cylinders (HEX) and body center cubic spheres (BCC), among others.[8,9] Self-consistent field theory (SCFT)[8] and the Random Phase Approximation (RPA)[10] have emerged as powerful tools for understanding the relationship between molecular structure, interactions, and phase behavior in conventional (uncharged) block copolymers.

It has been shown experimentally that the addition of salt affects the phase behavior of block copolymers.[11–15] Several theoretical groups have worked on the underpinnings of these observations.[16–20] The thermodynamics of these systems are affected by several factors that are not included in theoretical studies of conventional block copolymers. These factors include electrostatic interactions, charge dissociation, ion solvation, and physical cross-linking of chains due to the presence of ions. In early work, Wang and coworkers determined that ion solvation has the largest effect on the energetics of the block copolymer/salt system and added a term that they called “Born solvation energy” into a thermodynamic model.[16,21,22] This work suggests that the phase behavior of block copolymer/salt mixtures is similar to that of conventional block copolymers, provided χ is replaced by an effective interaction parameter, χ_{eff}, which accounts for the solvation energy contribution. In the simplest case, χ_{eff} increases linearly with salt concentration according to:

$$\chi_{eff} = \chi_0 + mr \quad (1)$$

where χ_0 is the Flory-Huggins interaction parameter of the neat system, r is the salt concentration given by $r =$ ¿¿ and m is a proportionality constant. This form for χ_{eff} was anticipated nearly three decades ago in the pioneering experimental studies by Mayes et al.[23] More recent theoretical work that accounts for salt-induced physical crosslinking indicates that Equation 1 still holds, although m must be redefined to account for the coupled and non-additive effects of ion-crosslinking and solvation energy.[24]

Theoretical work by de la Cruz and coworkers uses SCFT in conjunction with a hybrid liquid-state theory to account for electrostatic interactions in ion-containing copolymers.[25–27] We refer to this theory as Ionic-SCFT. This theory attempts to correct for charge ordering induced by ion correlations by explicitly adding an electrostatics term in conjunction with χ_0.[27] The surprising conclusion of this work is that the phase behavior of ion-containing block copolymers is qualitatively different from that of conventional block copolymers. In particular, the ordered phase window at low values of $\chi_0 N$ contains a "chimney" at low values of f_A (where A is the ionic block).[28] In polymers with low dielectric constants, such as PS and PEO, ordered phases with inverted morphologies (e.g. cylinders of B in a matrix of A) are predicted in the chimney.[26] We note that the phase diagram of conventional block copolymers is devoid of any chimney-like feature.

The purpose of this paper is to present experimental data on the phase behavior of SEO/LiTFSI mixtures in the vicinity of the order-disorder transition. The chain lengths of the SEO block copolymers were chosen so that the systems were disordered in the neat state. The volume fractions of the PEO blocks in our neat copolymers cover the range, $0.18 \leq f_{EO} \leq 0.84$, and focus on compositionally asymmetric systems ($f_{EO} \neq f_{PS} \neq 0.50$) to supplement previous work on symmetric systems.[11] The ordered morphologies that emerged upon the addition of salt were determined primarily by small angle X-ray scattering (SAXS). Our data enables a critical examination of theories described above.

Experimental Section:

Polymer Synthesis and Characterization:

The SEO copolymers in this study were synthesized, purified and characterized using methods described in refs 11,29. In this study, the polymers are named SEO (*xx*-*yy*), where *xx* and *yy* are the number-averaged molecular weights of PS, M_{PS}, and PEO, M_{PEO}, in kg mol^{-1}. The volume fractions of each block of the copolymers are given by

$$f_{EO} = \frac{\nu_{EO}}{\nu_{EO} + \frac{M_{PS} M_{EO}}{M_S M_{PEO}} \nu_S} \qquad (2)$$

where ν_{EO} and ν_S are the molar volumes of ethylene oxide and styrene monomer units, and M_{EO} and M_S are the molar masses of ethylene oxide (44.05 g mol^{-1}) and styrene (104.15 g mol^{-1}). M_{PS} and M_{PEO} are the number

averaged molecular weights of the PS and PEO blocks in kg mol^{-1}. Molar volumes were calculated by $\nu = M/\rho$. In this study, the densities of the PEO and PS blocks were given by $\rho_{PEO} = 1.139 - 7.31 \times 10^{-4} \times T$ and $\rho_{PS} = 1.08665 - 6.19 \times 10^{-4} \times T + 1.36 \times 10^{-7} \times T^2$.[11] The overall degree of polymerization, N, was calculated by $N = N_{PS} + N_{PEO}$ where

$$N_i = \frac{M_i}{\rho_i(T) N_A \nu_{ref}} \quad (3)$$

and N_A is Avogadro's number and ν_{ref} was fixed at 0.1 nm^3. Table 1 contains polymer characteristics, including the polydispersity indices, of the block copolymers in this study. The neat copolymers are completely transparent and colorless.

Table 1: Characteristics of polymers used in this study. N and f_{EO} were calculated at 140 °C.

Polymer	M_{PS} (kg mol^{-1})	M_{PEO} (kg mol^{-1})	f_{EO}	N
SEO(17.4-3.9)	17.4	3.9	0.18	350
SEO(9.4-2.4)	9.4	2.4	0.20	194
SEO(9.4-4.0)	9.4	4.0	0.29	220
SEO(3.8-8.2)	3.8	8.2	0.68	195
SEO(5.1-12.8)	5.1	12.8	0.72	291
SEO(4.0-22.4)	4	22.4	0.85	428
SEO(1.9-0.8)	1.9	0.8	0.29	47
SEO(1.4-1.6)	1.4	1.6	0.52	52
SEO(1.7-1.4)	1.7	1.4	0.44	54
SEO(2.9-3.3)	2.9	3.3	0.52	108
SEO(4.9-5.5)	4.9	5.5	0.52	181
SEO(16-16)	16.0	16.0	0.49	556

Data for SEO(1.9-0.8), SEO(1.4-1.6), SEO(1.7-1.4), SEO(2.9-3.3), SEO(4.9-5.5) are taken from a previous publication (ref. [30]) and data for SEO(16-16) are taken from ref [31].

Electrolyte Preparation

The salt-containing copolymers were prepared using methods described in ref [32]. Due to the hygroscopic nature of the salt, Argon environment gloveboxes (Vacuum Atmosphere Company) with low oxygen and water levels were used for all sample preparation. The molar ratio of lithium ions to ethylene oxide (EO) moieties, *r,* is used in this study to

quantify salt concentration. The number of EO units per polymer chain is calculated from M_{PEO} without correcting for end groups. We assume that the all of the salt resides in the PEO domain [33–35] and determine the volume fraction of the salty PEO domain by

$$f_{EO,salt} = \frac{\nu_{EO,salt}}{\nu_{EO,salt} + \left(\frac{M_{PS}M_{EO}}{M_S M_{PEO}}\right)\nu_S} \quad (4)$$

where $\nu_{EO,salt}$ is the molar volume of salt-containing PEO calculated by $\nu_{EO,salt} = \frac{M_{PEO}}{\rho_{EO,salt}(r)}$ where $\rho_{EO,salt}(r)$ is taken from ref 5. By using the measured density of salty PEO, we have accounted for the volume change of mixing within the PEO-rich domains. We assume that the monomer volume of PS is unaffected by the addition of salt; measured densities SEO(XX)/LiTFSI mixtures (Jenna's polymer – if it is not in our Table write a little note) indicated that this is an excellent assumption. A full list of properties for the salt-containing samples used in this study can be found in Table 2.

Small Angle X-Ray Scattering (SAXS) Measurements

SAXS samples were prepared by and thermally pre-treated according to methods described in ref [36]. SAXS measurements were conducted at the Advanced Light Source beamline 7.3.3 at Lawrence Berkeley National Lab[37] and Stanford Synchrotron Radiation Light Source beamline 1-5 at SLAC National Accelerator Laboratory. In order to compare data collected at each beamline, temperature calibrations were conducted to measure the absolute

temperature of the samples by making separate electrolyte samples with a thermocouple running through the sample holder. The data presented in the main text reflects the absolute temperatures of the samples. Silver behenate was used to determine the beam center and sample-to-detector distance. The scattered intensity was corrected for beam transmission, empty cell scattering, as well as for unavoidable air gaps in the system. Two-dimensional scattering patterns were integrated azimuthally using the Nika program for IGOR Pro to produce one-dimensional scattering profiles.[38] Measurements were taken in a custom-built 8-sample heating stage, starting at 132 °C and cooling in steps of about 10 °C to 75 °C. Samples were annealed for about 30 min at each temperature before taking measurements.

Depolarized Light Scattering (DPLS)

The samples for DPLS were prepared like SAXS samples but were sealed between quartz windows in custom-designed airtight aluminum sample holders.[39] The light source was a continuous-wave diode laser with a wavelength of 633nm and an output power adjustable from 0 to 40mW. The sample was placed between crossed polarizers in a heating block that was electrically heated by two heating elements, and the temperature of the sample was controlled by an Omega Engineering temperature controller (CN9111A).[40] In order to determine the order-disorder transition temperature (T_{odt}) of the sample, the birefringence method was employed.[41] In the order-to-disorder experiments, the total depolarized transmitted laser power was

obtained as the sample was heated in approximately 10 °C increments from 80 °C to 110 °C. When the sample temperature is higher than the T_{odt}, the sample is completely disordered, and the total power decays to zero. At the end of every temperature step, a DPLS scattering pattern was captured with a CCD camera. For the coexistence experiments, the samples were heated to 80°C and the scattering patterns were recorded after 40 minutes at 80 °C. All scattering patterns were stored as 8-bit, 801 x 801 pixel TIFF image files. The intensity at each pixel was represented by a dimensionless number between 0 and 255. The total depolarized transmitted power was calculated from the image file by summing the intensities at every pixel, after subtracting a background noise image taken with a completely disordered sample.

Table 2: Characteristics of asymmetric SEO/LiTFSI mixtures used in this study

Polymer	r	$f_{EO,salt}$	Morphology	T_{odt}
SEO(5.1-12.8)	0.000	0.70	DIS	
	0.005	0.71	DIS	
	0.010	0.71	DIS to LAM	101 °C
	0.025	0.72	GYR	
	0.050	0.73	HEX	
	0.075	0.74	HEX	
	0.100	0.75	HEX	
	0.150	0.77	HEX	
	0.200	0.79	HEX	
	0.250	0.81	HEX	
	0.300	0.82	HEX	
SEO(4.0-22.4)	0.000	0.84	DIS	
	0.005	0.84	DIS	
	0.010	0.84	DIS	
	0.025	0.85	HEX	
	0.050	0.86	HEX	
	0.075	0.87	HEX/BCC	
	0.100	0.87	HEX/BCC	
	0.150	0.88	BCC	
	0.200	0.89	BCC	
	0.250	0.90	BCC	
	0.300	0.91	BCC	
SEO(3.8-8.2)	0.000	0.67	DIS	
	0.005	0.67	DIS	
	0.010	0.68	DIS	
	0.025	0.69	DIS to LAM	127 °C
	0.050	0.70	GYR	
	0.075	0.71	HEX	
	0.100	0.73	HEX	
	0.150	0.75	HEX	
	0.200	0.76	HEX	
	0.250	0.78	HEX	
	0.300	0.79	HEX	
SEO(9.4-2.4)	0.000	0.19	DIS	
	0.005	0.20	DIS	
	0.010	0.20	BCC/BCC	
	0.025	0.21	DIS	
	0.050	0.22	HEX	
	0.075	0.23	HEX	
SEO(9.4-4.0)	0.000	0.29	DIS	
	0.005	0.29	DIS	
	0.010	0.29	HEX	
	0.025	0.30	HEX	
	0.050	0.32	HEX	
	0.075	0.33	HEX	
	0.100	0.34	HEX	
	0.150	0.37	HEX	
	0.200	0.39	HEX	
	0.250	0.41	HEX	
	0.300	0.43	HEX	
SEO(17.4-3.9)	0.000	0.17	DIS	
	0.005	0.18	BCC	
	0.010	0.18	BCC	
	0.025	0.18	BCC	
	0.050	0.20	BCC	
	0.075	0.21	BCC	

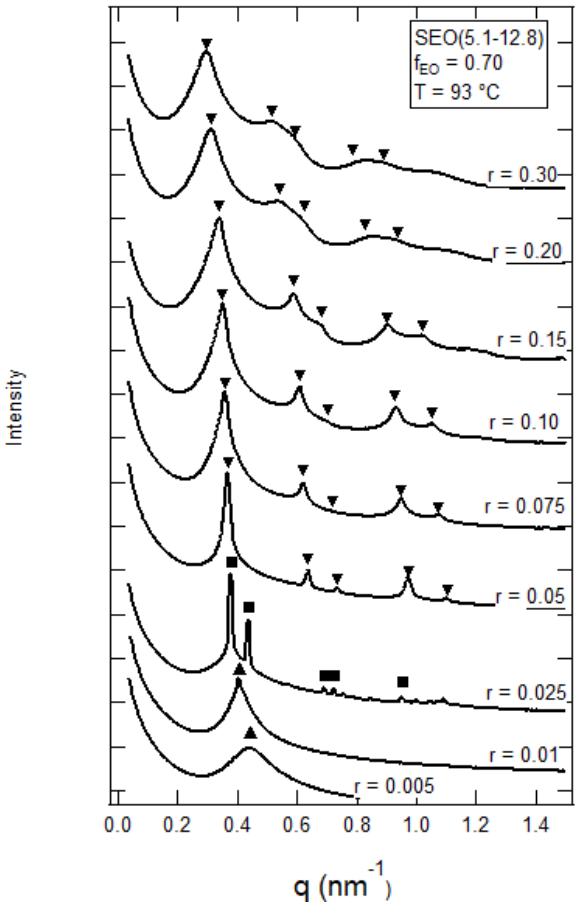

Figure 1: SAXS profiles at 93 °C for SEO(5.1-12.8) at several salt concentrations. Profiles are offset vertically for clarity. The symbols represent the primary and higher order scattering peaks: , , and represent HEX, GYR, and DIS phases respectively.

Results and Discussion

Table 2 outlines the polymer characteristics and phase behavior for all salt-containing SEO copolymer samples. All six SEO copolymers are disordered in the neat state and SAXS profiles of the neat copolymers can be found in the Supporting Information (Figure S1). Figure 1 shows the SAXS profiles for SEO(5.1-12.8) at 93 °C for salt concentrations ranging from

$0.005 \leq r \leq 0.300$. At the lowest salt concentration, r = 0.005, the electrolyte exhibits a single broad disordered peak at q^* = 0.433 nm^{-1}, where q^* is the location of the primary peak. At r = 0.01, the sample exhibits a weak signature of order; note the presence of a small, but noticeable, sharp primary peak at q = 0.444 nm^{-1} superimposed on a broad peak characteristic of a disordered phase. Upon further salt addition to r = 0.025, the sample forms a GYR state with higher order reflections at $\frac{q}{q^*} = \sqrt{\frac{4}{3}}, \sqrt{\frac{8}{3}}$ and $\sqrt{\frac{11}{3}}$. At all higher salt concentrations, $0.025 \leq r \leq 0.30$, the electrolytes are in the HEX state with higher order reflections at $\frac{q}{q^*} = \sqrt{3}, \sqrt{4}, \sqrt{7}$ and $\sqrt{9}$.

SAXS was also conducted on all salt concentrations of SEO(5.1-12.8) from $75\,℃ \leq T \leq 132\,℃$ in approximately 10 °C increments. Only the sample with r = 0.01 shows temperature-dependent phase behavior. SAXS profiles of this sample at selected temperatures are shown in Figure 2a. At 85 °C, we see the scattering signature of LAM. At 93 °C, we see the scattering signature of coexisting LAM and DIS phases. At 113 °C, we see a pure DIS phase. The order-to-disorder transition in this sample was also studied by birefringence (Figure 2b). At temperatures below 87 °C, the birefringence signal is more or less independent of temperature. At temperatures between $87\,℃ \leq T \leq 101\,℃$, the birefringence signal decreases smoothly to zero. We therefore determined the order-disorder transition temperature, T_{odt}, to be

101 °C.[41] The smooth decrease is consistent with the presence of coexisting LAM and DIS phases in this temperature window, which has been seen previously in block copolymer salt mixtures.[32,42] Only the LAM phase contributes to the birefringence signal and the fraction of the sample occupied by the LAM phase decreases with increasing temperature and vanishes at T_{odt}.[43]

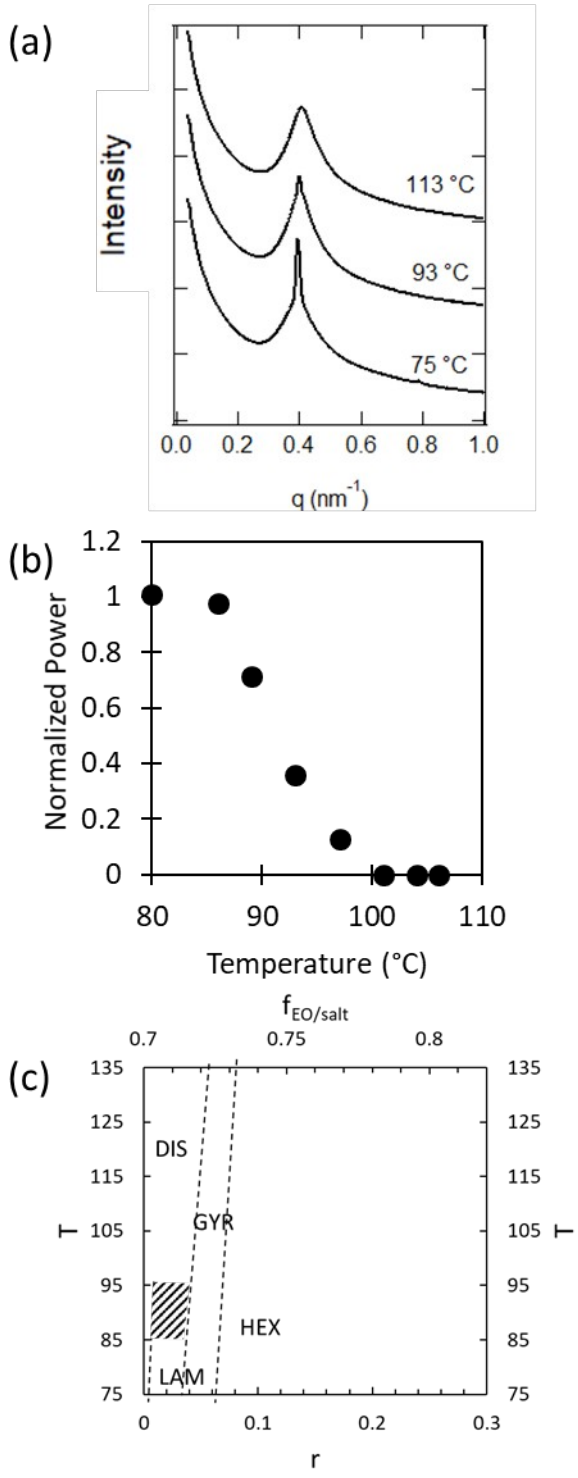

Figure 2: (a) SAXS profiles of SEO(5.1-12.8) r = 0.01 at different temperatures through the order-disorder transition (b) Plot of normalized power versus temperature from birefringence measurements to determine the T_{odt} of the sample (c) Phase diagram of SEO(5.1-12.8) as a function of

temperature and salt concentration. Dashed lines mark phase boundaries and the hatched region indicate coexistence between phases.

The phase behavior of salty SEO(5.1-12.8) is shown in Figure 2c as a function of temperature and salt concentration. The dashed lines represent the boundaries between two phases and the hatched pattern indicates coexistence between DIS and LAM. Phase boundaries are placed to bisect known phases when the coexistence window was not observed. The Gibbs phase rule requires coexistence across all phase boundaries,[15,42,44,45] however, the step-changes in salt concentration and temperature were too large to observe coexistence in most cases. We have chosen to omit the individual data points interpreted from SAXS to focus on the overall phase behavior.

Figure 3a shows the SAXS profiles for SEO(4.0-22.4) at 93 °C. SEO(4.0-22.4) is the most asymmetric and longest polymer studied with f_{EO} = 0.84 and N = 428. It remains disordered at $r \leq 0.01$ before forming HEX at $0.025 \leq r \leq 0.05$ with higher order reflections at $\frac{q}{q^*} = \sqrt{3}$ and $\sqrt{4}$. At $0.075 \leq r \leq 0.10$, we see coexistence between HEX (open triangles) and BCC phases (filled diamonds). The presence of both filled and open symbols in Figure 3a indicates coexistence between two ordered phases. At a salt concentration of r = 0.075, the primary peak for the HEX phase appears at q^* = 0.324 nm^{-1} and that of the BCC phase at q^* = 0.347 nm^{-1}. The HEX phase has a larger

domain spacing, given by $d=\frac{2\pi}{q^*}$, than the BCC phase: 19.4 nm versus 18.1 nm, respectively. The higher order reflections for the BCC phase are seen at $\frac{q}{q^*}=\sqrt{2},\sqrt{3},\sqrt{4}$, and $\sqrt{6}$. The relative intensities of the peaks associated with HEX and BCC morphologies change with salt concentration; for example, at r = 0.075, HEX is the majority component of the system and at r = 0.10, BCC becomes the majority phase. Since the HEX phase is optically anisotropic and the BCC phase is optically isotropic, the gradual transition from HEX to BCC with salt concentration can be studied by birefringence.[46] The dependence of the birefringence signal on salt concentration at 80 °C in the HEX/BCC coexistence window is given in the Supporting Information (Figure S2). The normalized signal decreases smoothly over a wide range of salt concentration to a value of 0.02 at r = 0.15, where only spheres are seen. The reason for obtaining the small signal from BCC remains to be established. It may arise from strain trapped within the sample as it was prepared. At the highest salt concentrations, $r \geq 0.15$, SEO(4.0-22.4) forms a pure BCC phase. The phase behavior of SEO(4.0-22.4) is independent of temperature at all salt concentrations.

Figure 3b shows the observed phase behavior of salty SEO(4.0-22.4) as a function of temperature and salt concentration. Dashed lines represent phase boundaries between morphologies and the hatched region represents coexistence of BCC and HEX phases. In this coexistence window, salt must

be partitioned between these two phases. Based on the location of the coexistence window, we anticipate that the salt concentration is higher in regions where the BCC phase is found.

The phase behavior of SEO(3.8-8.2) is similar to that of SEO(5.1-12.8) and SAXS data obtained from this sample is shown in Supporting Information (Figure S3). The phase behavior for SEO(9.4-2.4), SEO(9.4-4.0) and SEO(17.4-3.9) has been previously reported in ref [36].

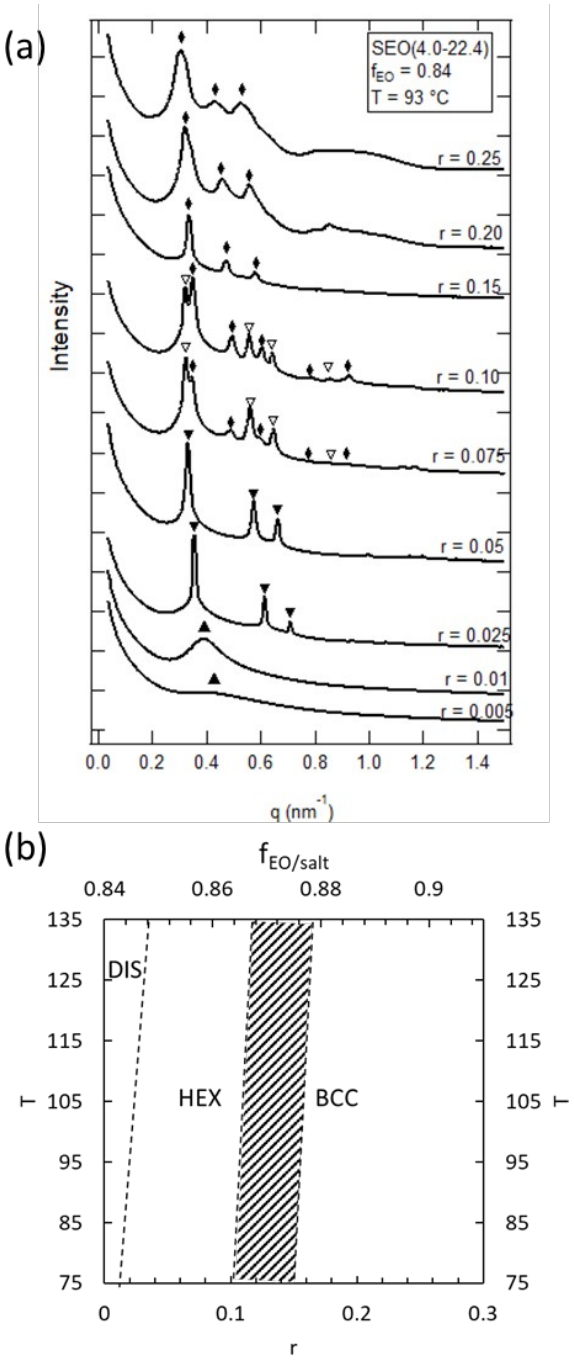

Figure 3: (a) SAXS profiles at 93 °C for SEO(4.0-22.4) at several salt concentrations. Profiles area offset vertically for clarity. The symbols represent the primary and higher order scattering peaks: ▲, ♦ and ▼ represent HEX, BCC, and DIS phases respectively. (b) Phase diagram of SEO (4.0-22.4)/LiTFSI as a function of salt concentration and temperature. Dashed lines mark phase boundaries and the hatched region indicate coexistence.

It is evident from the discussion above that the phase behavior of SEO/LiTFSI mixtures is a complex function of chain length, copolymer composition, salt concentration and temperature. Our objective is to compare our findings with prevailing theories directly. There are no established approaches for accomplishing this. The phase behavior of conventional block copolymers is usually reported on a χN versus f_A plot where χN reflects segregation strength. However, there is much debate in the literature about the relationship between experimentally determined χ and that demanded by theory.[47–50] Many more questions arise in the case of salty block copolymers wherein χ must be replaced by χ_{eff}.[21] If we assume that χ_{eff} for block copolymer/salt mixtures can be approximated by Equation 1, then the segregation strength in these mixtures is approximated as

$$\chi_{eff} N = \chi_0 N + mrN \quad (5)$$

Note that the segregation strength is proportional to the product Nr.

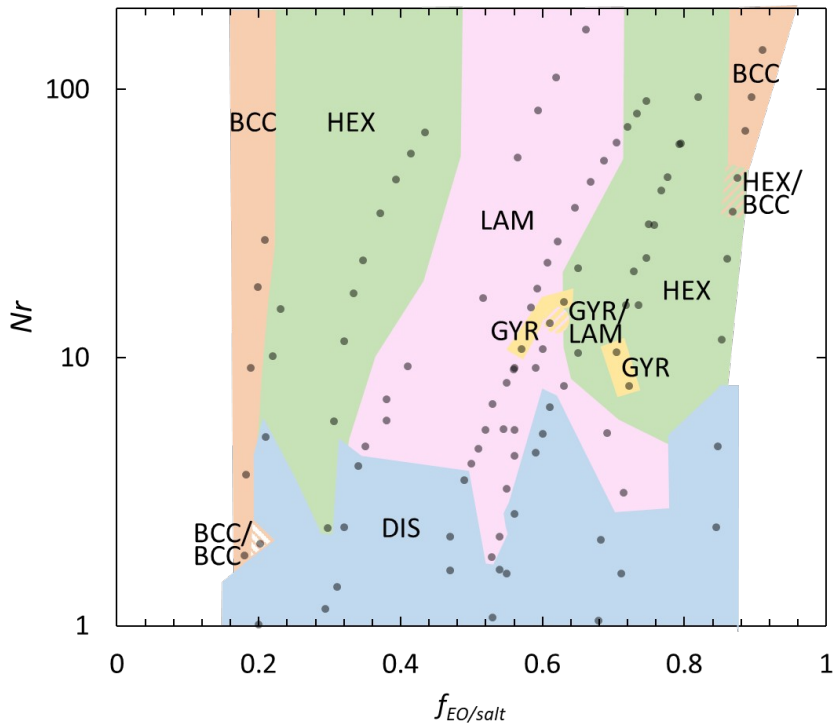

Figure 4: Morphology data for SEO/LiTFSI copolymers at 100 °C plotted as a function of *Nr* versus volume fraction of the salt containing phase, $f_{EO,salt}$. Gray symbols indicate a discrete sample where morphology was determined through SAXS. Phase boundaries were drawn to bisect known morphologies where no window of coexistence was observed. Coexistence is denoted by hatched colored regions.

As a first step, we present the phase behavior of all of the samples described above at 100 °C in Figure 4, where the product *Nr* is now used to represent the segregation strength and $f_{EO,salt}$, the volume fraction of the salt-containing PEO-rich microphase, is used to quantify composition. Also included in this figure is the phase behavior of nearly-symmetric SEO/LiTFSI mixtures at 100 °C reported in ref [11,51]. ~~In principle, we could use the product $\chi_{eff}N$ to quantify segregation strength, but this would involve assumptions~~

~~such as the value of χ_0 and the validity of Equation 5 across all compositions.~~ In Figure 4, phase boundaries are drawn to bisect the known morphologies when no coexistence is seen between phases. Regions of coexistence are denoted by the hatched pattern of the colors indicative of the two observed morphologies. Due to the broad range of Nr covered in this study, a log scale is used on the y-axis in Figure 4. Neat samples (r = 0) are therefore omitted from the phase diagram. ~~Although Nr is only mathematically proportional to the segregation strength, we can create a phase diagram that closely resembles a χN vs f_A phase diagram.~~ Note that the dominant morphologies (BCC, HEX, LAM and DIS) are obtained in contiguous regions on the Nr vs $f_{EO,salt}$ plot. We see the DIS phase across all compositions at low values of Nr. The LAM phase is seen in the range of $0.4 < f_{EO,salt} < 0.6$, flanked by HEX phases on either side, which are in turn flanked by BCC phases. Two separate pockets of the GYR phase are found in the vicinity of LAM/HEX border. It is important to recognize that in Figure 4 we have succeeded in organizing a large body of morphological data that is dependent on three independent parameters – N, r, f_{EO} – using just two parameters. We note that the is no evidence of a chimney region predicted in ref. x at low values of $f_{EO,salt}$.

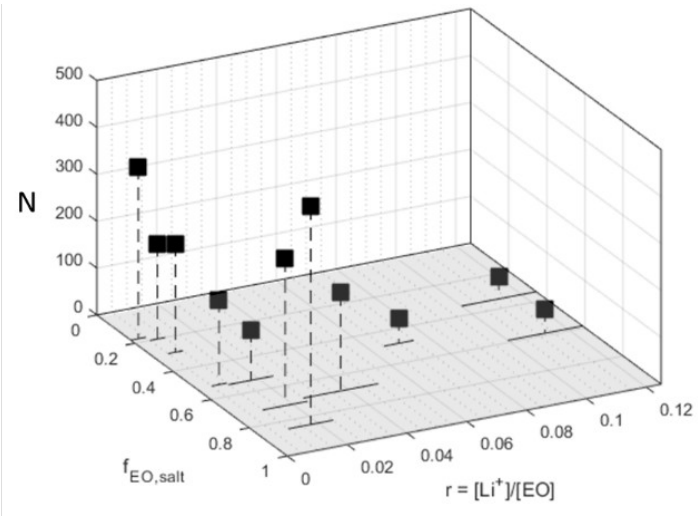

Figure 5: Chain lengths, N, at the order-disorder transition at Cversus polymer composition and ion concentration for the SEO/LiTFSI system.

For a given system characterized by N and f_{EO}, we have determined the critical salt concentration beyond which ordered phases are observed at 100 °C. This information is conveyed in Figure 5 where N is plotted as a function of r and $f_{EO,salt}$ on a three-dimensional plot. The step change in salt concentration that leads to order formation is used as the error bar on the $N=0$ plane. As expected, shorter polymers order at higher salt concentrations. However, it is evident that the surface demarcating the order-to-disorder transition in N-r-$f_{EO,salt}$ space, the surface obtained by connecting the squares in Figure 5, is complex.

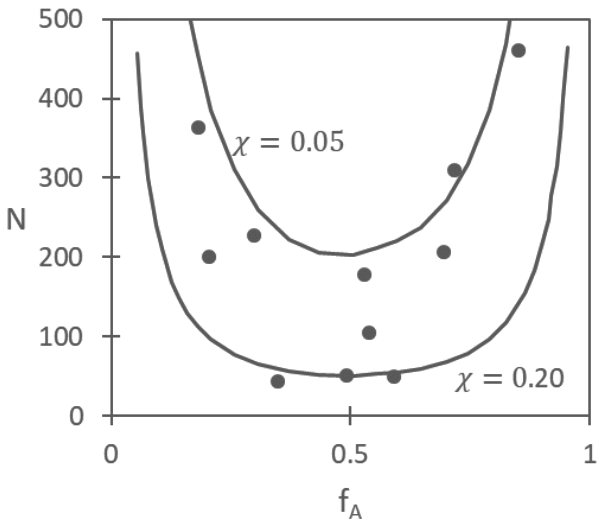

Figure 6: Chain length, N, at the order-disorder transition as a function of volume fraction for the ion-containing phases (filled circles are SEO/LiTFSI) and SCFT for conventional block copolymers at χ=¿ 0.20 and 0.05 (solid lines).

Cochran and Fredrickson have computed the boundary between ordered and disordered phases in neat block copolymers using SCFT.[7] They expressed their results on a χN vs f_A plot. We are interested in the relationship between N and f_A at a fixed temperature, or χ. Our objective is to compare the data presented in Figure 5 with the Cochran and Fredrickson predictions. In our experiments, the order-to-disorder transition was located over a range of $0.0025 < r < 0.125$. Over this range, χ_{eff} values reported in the literature range between 0.05 and 0.20.[11] In order to make connections between the Cochran-Fredrickson SCFT and experiments, we calculate N at the order-disorder transition as a function of f_A using these two values for χ. The results of these calculations are the two U-shaped curves in Figure 6. The symbols in Figure 6 represent the experimental SEO/LiTFSI systems in which salt-induced order-disorder transitions have been identified taken from

Figure 5. Generally, the experimental data points lie between the two SCFT curves and are consistent with SCFT. Figure 6 indicates that the phase behavior of salty SEO mixtures can be mapped on to the phase behavior of uncharged block copolymers.

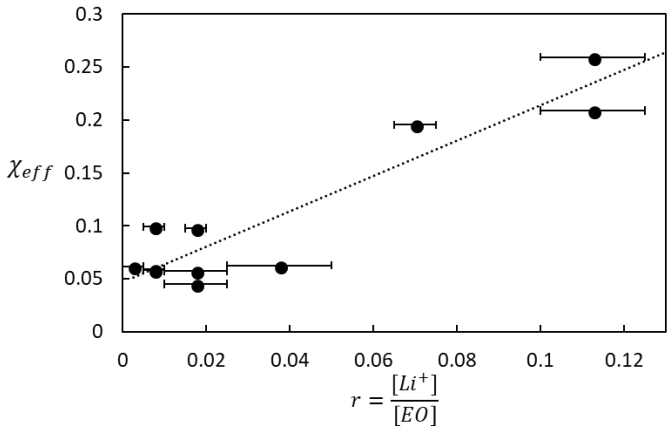

Figure 7: Calculated χ_{eff} from SCFT as a function of *r* for the salty SEO copolymers using the composition dependence of the order-disorder transition (equation 7) at 100 ºC. The data are consistent with $\chi_{eff}=\chi_0+mr$ with $\chi_0=0.047$ and $m=1.67$. The error bars represent the step change in salt concentration that leads to order formation.

We use the experimentally measured locations of the order-disorder transitions and the Cochran-Fredrickson (ref [7]) SCFT to estimate χ_{eff}. The Cochran-Fredrickson SCFT results for the order-disorder phase boundary can be recast in the form

$$(\chi N)_{ODT}=g(f_A)=10.495+C_1(f_A-0.5)^2+C_2(f_A-0.5)^4+C_3(f_A-0.5)^6+C_4(f_A-0.5)^8 \quad (6)$$

(The fit and coefficient values are given in Figure S4). For a given SEO/salt mixtures, the value of χ at the order-disorder transition was calculated using eq. 6 with the assumption that $f_A = f_{EO,salt}$, to obtain

$$\chi_{eff} = \frac{10.495 + C_1\left(f_{EO,salt} - 0.5\right)^2 + C_2\left(f_{EO,salt} - 0.5\right)^4 + C_3\left(f_{EO,salt} - 0.5\right)^6 + C_4\left(f_{EO,salt} - 0.5\right)^8}{N} \quad (7)$$

This enables taking each data point in Figure 5 where N at the ODT is given as a function of $f_{EO,salt}$ and r, and converting it into χ_{eff} for the given value of r. Our approach for determining χ_{eff} is similar to the time-honored method of determining phase boundaries in binary polymer solutions and blends and mapping these results onto the predictions of the Flory-Huggins theory to determine the interaction parameter.[50,52,53] The calculated values of χ_{eff} thus obtained are plotted versus salt concentration, r, in Figure 7. The estimates for χ_{eff} show a strong linear dependence with r, consistent with Equation 1. A least-squares fit through the data in Figure 7 gives $\chi_0 = 0.047$ and $m = 1.67$. These values match experimentally determined values of χ_0 and m in ref 15, where χ_{eff} was determined from RPA fits through SAXS data obtained from the disordered state. It is important to note that the salt concentration, r, is not explicitly used when determining χ_{eff}. The applicability of a linear relationship between χ_{eff} and r over a wide salt concentration ($0.005 \le r \le 0.10$) and EO volume fractions ($0.18 \le f_{EO} \le 0.84$) is noteworthy. In spite of these complexities, our work

indicates that most of the important features of the SEO/LiTFSI phase diagram can be reproduced by combining the linear relationship in Fig. 7 with conventional block copolymer SCFT.

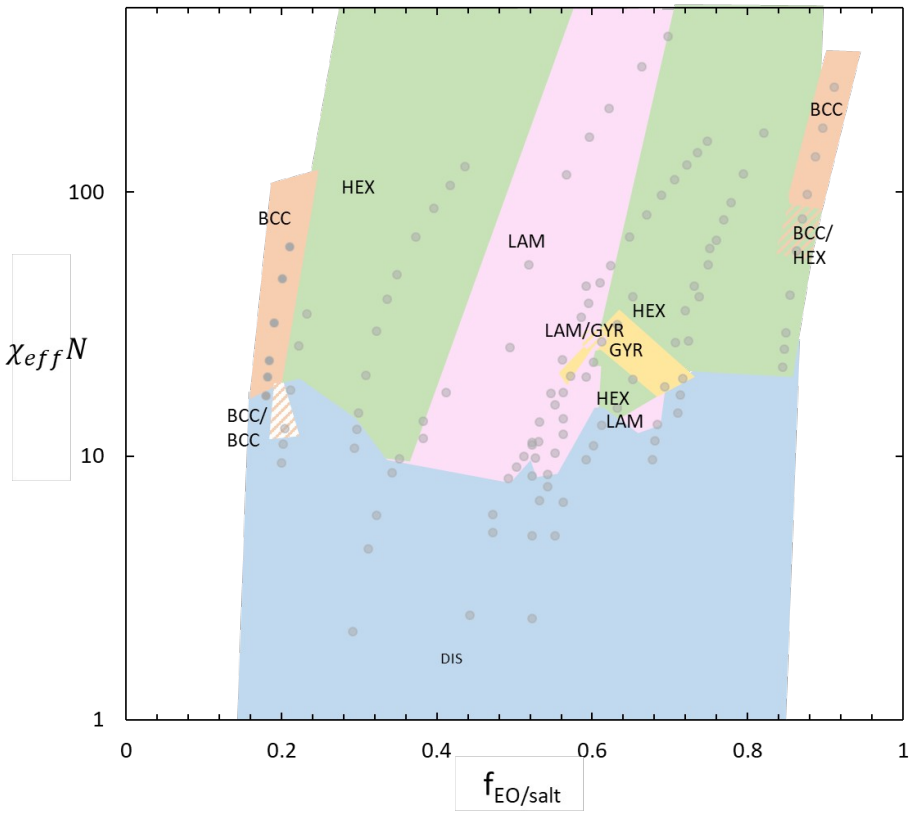

The particular constants (0.047 and 1.67 in equation (8)) used to quantify the effective segregation strength between the blocks in the presence of salt. If, for example, these constants are replaced by XX and YY, the morphologies appear scrambled on the phase diagram. The boundaries between different morphologies in SEO/LiTFSI are straight but tilted to the right when plotted on a semi-log $\chi_{eff}N$ versus $f_{EO,salt}$ plot. The appearance of small coexistence windows at the bottom of the BCC phases at both low and high

$f_{EO,salt}$ values is clearly due to the presence of salt; they are not observed in conventional block copolymers. Aside from these differences, the phase behavior of SEO/LiTFSI is similar to that of conventional block copolymers.

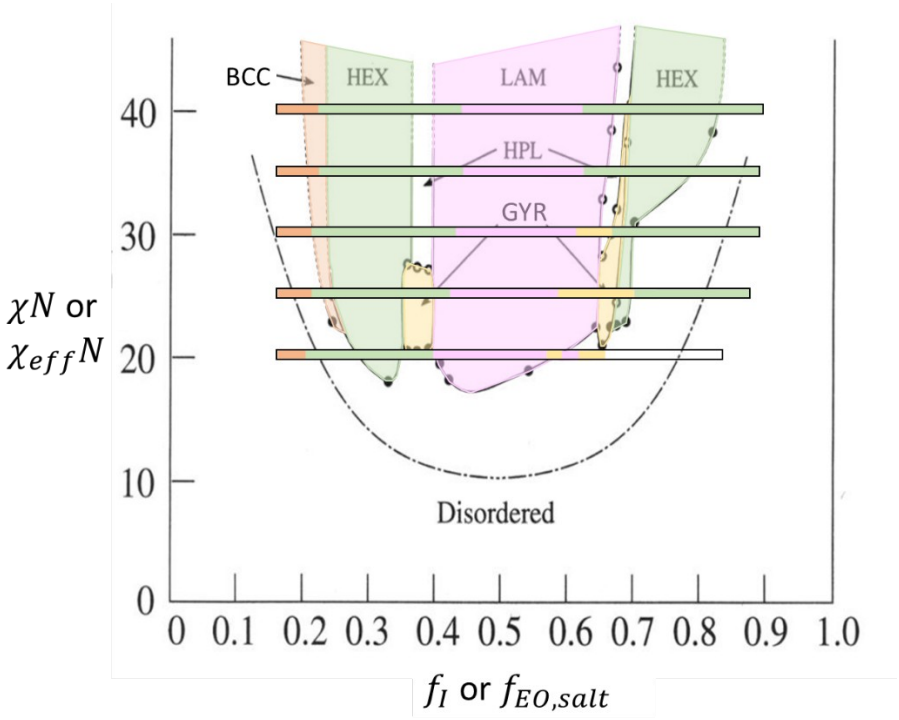

Figure 9: Phase behavior diagram of SIP reproduced from Khandpur et al. The five colored bars represent the phase behavior of SEO/LiTFSI taken from Figure 8. The colors match the morphologies labeled in Figure 8 with the DIS phase left unlabeled in white.

The similarity of SEO/LiTFSI phase behavior and that of conventional block copolymers is depicted in Figure 9 which shows the phase diagram of a neat conventional block copolymer, polystyrene-block-polyisoprene (SIP), taken from ref [54]. We have colored all of the ordered phases that are relevant to the present study (LAM, HEX, BCC and GYR) using the same color scheme as Figure 8. The x-axis in Figure 9 is the volume fraction of the polyisoprene

(PI) block and the y-axis is χN for SIP. Also shown in Figure 9 are five colored horizontal bars evenly spaced between $20 \leq \chi_{eff} N \leq 40$. These bars present the phase behavior of SEO/LiTFSI mixtures (Figure 8) with $\chi_{eff} N$ as the ordinate and $f_{EO,salt}$ as the abscissa. Within each bar, the color represents the ordered phase using the same color scheme as Figure 8 (the DIS phase is not colored). It is clear from Figure 9 that the phase behavior of salty block copolymers closely resembles that of conventional block copolymers. It does not contain a chimney-like feature that was predicted by ionic SCFT.(ref) The BCC phase is found at low values of segregation strength (25) for styrene-rich (S-rich) block copolymers in both SIP and SEO/LiTFSI. In both IP-rich and EO-rich systems, the BCC phase is absent at values of segregation strength as high as 40. This similarity is noteworthy given the differences between PI and PEO/LiTFSI. The widths of the HEX phases in SEO/LiTFSI mixtures are similar in both S-rich and EO-rich systems, consistent with all of the theories on neat block copolymer self-assembly.[6] There is reasonable agreement between the widths of the LAM phases found in SIP and SEO/LiTFSI. The GYR pockets in SEO/LiTFSI are only found in the EO-rich side of the phase diagram. It is evident that underlying simplicity of the phase behavior of SEO/LiTFSI mixtures is revealed by simple rescaling χ to account for the additional interactions due to the presence of salt copolymer/salt mixtures.

Conclusions

There is continued interest in studying the effect of salt on the thermodynamics of block copolymers for both fundamental understanding of salt/copolymer mixtures as well as for applications such as solid-state battery separators. We present the phase behavior of SEO/LiTFSI systems over a wide range of compositions $0.18 \leq f_{EO,salt} \leq 0.84$. Data from weakly and strongly segregated systems are presented; salt concentration is used to tune segregation strength, which is approximated by the product Nr. The relationship between chain length, polymer composition, and salt concentration was examined at the order-to-disorder transition. Our experiments reveal a distinctly non-monotonic relationship between polymer composition and chain length at the order-disorder transition. A linear expression for the dependence of χ_{eff} on salt concentration is obtained by mapping the observed order-disorder phase boundary on to SCFT predictions for uncharged block copolymers. The phase behavior of SEO/LiTFSI mixtures, when plotted on a $\chi_{eff}N$ versus fPEO/salt plot is similar to that of a cN versus fA plot obtained for conventional block copolymers. The only difference is that the phase boundaries are not vertical; they tilt to the right. We hope that our work will allow for discrimination of different theoretical approaches that have been used to describe the effect of electrostatic interactions on block copolymer phase behavior.

ASSOCIATED CONTENT

Supporting Information.

Additional information on the synthesis and characterization of the block copolymer electrolytes are given in the Supporting Information.

AUTHOR INFORMATION

Corresponding Author

*(N.P.B) Email: nbalsara@berkeley.edu.

Author Contributions

The manuscript was written through contributions of all authors. All authors have given approval to the final version of the manuscript.

Notes

Any additional relevant notes should be placed here.

ACKNOWLEDGMENT

Primary funding for this work was provided by the National Science Foundation through Award DMR-1505444. Work for the birefringence experiments was provided by the National Science Foundation through Award DMR-1505476. Work at the Advanced Light Advanced Light Source, which is a DOE Office of Science User Facility, was supported by Contract No. DE-AC02-05CH11231. Work at the Stanford Synchrotron Radiation Light Source, a user facility at SLAC National Accelerator Laboratory, was supported by the

U.S. Department of Energy, Office of Science, Office of Basic Energy Sciences under Contract No. DE-AC02-76SF00515. W.S.L. acknowledges funding from the National Science Foundation Graduate Student Research Fellowship DGE-1106400.

ABBREVIATIONS

BCC	body center cubic
DPLS	depolarized light scattering
GYR	gyroid
HEX	hexagonally packed cylinders
LAM	lamellar
LiTFSI	lithium bis(trifluoromethanesulfonyl) imide salt
N_A	Avogadro's number
PEO	poly(ethylene oxide)
PI	polyisoprene
PS	polystyrene
RPA	Random Phase Approximation
SAXS	small angle X-ray scattering
SCFT	Self Consistent Field Theory
SEO	polystyrene-*block*-poly(ethylene oxide)
SIP	polystyrene -*block*-polyisoprene
T_{odt}	order-disorder temperature

LIST OF SYMBOLS

d	domain spacing (nm)
$f_{EO,salt}$	volume fraction of the PEO/LiTFSI phase
f_A	volume fraction of species A
f_{EO}	volume fraction of PEO phase
f_q	fraction of charged species
f_S	volume fraction of PS phase
M_{PEO}	number-averaged molecular weight of the PEO block (kg mol^{-1})
M_{PS}	number-averaged molecular weight of PS block (kg mol^{-1})
N	number-averaged degree of polymerization (sites chain^{-1})
q	scattering vector (nm^{-1})

q^*	scattering vector at the primary peak (nm^{-1})
r	salt concentration ($[Li^+]\ [EO]^{-1}$)

Greek

Γ	electrostatic cohesion parameter
ε	conformational asymmetry parameter
ϵ_i	dielectric constant of species i
ν_i	molar volume of species i ($cm^3\ mol^{-1}$)
ν_{ref}	reference volume ($nm^3\ site^{-1}$)
ρ_i	density of species i ($g\ cm^{-3}$)
χ	Flory-Huggins interaction parameter
χ_{eff}	effective Flory-Huggins interaction parameter

References:

(1) Soo, P. P.; Huang, B.; Jang, Y.-I.; Chiang, Y.-M.; Sadoway, D. R.; Mayes, A. M. Rubbery Block Copolymer Electrolytes for Solid-State Rechargeable Lithium Batteries. *J. Electrochem. Soc.* **1999**, *146* (1), 32–37.

(2) Young, W. S.; Kuan, W. F.; Epps, T. H. Block Copolymer Electrolytes for Rechargeable Lithium Batteries. *J. Polym. Sci. Part B Polym. Phys.* **2014**, *52* (1), 1–16.

(3) Singh, M.; Odusanya, O.; Wilmes, G. M.; Eitouni, H. B.; Gomez, E. D.; Patel, a J.; Chen, V. L.; Park, M. J.; Fragouli, P.; Iatrou, H.; et al. Effect of Molecular Weight on the Mechanical and Electrical Properties of Block Copolymer Electrolytes. *Macromolecules* **2007**, *40* (13), 4578–4585.

(4) Hallinan, D. T.; Balsara, N. P. Polymer Electrolytes. *Annu. Rev. Mater. Res* **2013**, *43*, 503–525.

(5) Pesko, D. M.; Timachova, K.; Bhattacharya, R.; Smith, M. C.; Villaluenga, I.; Newman, J.; Balsara, N. P. Negative Transference Numbers in Poly(Ethylene Oxide)-Based Electrolytes. *J. Electrochem. Soc.* **2017**, *164* (11), E3569–E3575.

(6) Bates, F. S.; Fredrickson, G. H. Block Copolymer Thermodynamics: Theory and Experiment. *Annu. Rev. Phys. Chem.* **1990**, *41* (1), 525–557.

(7) Cochran, E. W.; Garcia-Cervera, C. J.; Fredrickson, G. H. Stability of the Gyroid Phase in Diblock Copolymers at Strong Segregation. *Macromolecules* **2006**, *39* (7), 2449–2451.

(8) Matsen, M. W.; Schick, M. Stable and Unstable Phases of a Diblock Copolymer Melt. *Phys. Rev. Lett.* **1994**, *72* (16), 2660–2663.

(9) Kawasaki, K.; Kawakatsu, T. Equilibrium Morphology of Block Copolymer Melts. *Macromolecules* **1990**, *23* (17), 4006–4019.

(10) Leibler, L. Theory of Microphase Separation in Block Copolymers. *Macromolecules* **1980**, *13* (10), 1602–1617.

(11) Teran, A. A.; Balsara, N. P. Thermodynamics of Block Copolymers with and without Salt. *J. Phys. Chem. B* **2014**, *118* (1), 4–17.

(12) Epps, T. H.; Bailey, T. S.; Waletzko, R.; Bates, F. S. Phase Behavior and Block Sequence Effects in Lithium Perchlorate-Doped Poly (Isoprene- b -Styrene- b -Ethylene Oxide) and Poly (Styrene- b -Isoprene- b -Ethylene Oxide) Triblock Copolymers. *Macromolecules* **2003**, *36* (8), 2873–2881.

(13) Irwin, M. T.; Hickey, R. J.; Xie, S.; Bates, F. S.; Lodge, T. P. Lithium Salt-Induced Microstructure and Ordering in Diblock Copolymer/Homopolymer Blends. *Macromolecules* **2016**, *49* (13), 4839–4849.

(14) Gunkel, I.; Thurn-Albrecht, T. Thermodynamic and Structural Changes in Ion-Containing Symmetric Diblock Copolymers: A Small-Angle X-Ray Scattering Study. *Macromolecules* **2012**, *45* (1), 283–291.

(15) Wanakule, N. S.; Virgili, J. M.; Teran, A. A.; Wang, Z. G.; Balsara, N. P. Thermodynamic Properties of Block Copolymer Electrolytes Containing Imidazolium and Lithium Salts. *Macromolecules* **2010**, *43* (19), 8282–8289.

(16) Nakamura, I.; Wang, Z.-G. Salt-Doped Block Copolymers: Ion Distribution, Domain Spacing and Effective χ Parameter. *Soft Matter* **2012**, *8* (36), 9356.

(17) Sing, C. E.; Olvera De La Cruz, M. Polyelectrolyte Blends and Nontrivial Behavior in

Effective Flory-Huggins Parameters. *ACS Macro Lett.* **2014**, *3* (8), 698–702.

(18) Ganesan, V.; Pyramitsyn, V.; Bertoni, C.; Shah, M. Mechanisms Underlying Ion Transport in Lamellar Block Copolymer Membranes. *ACS Macro Lett.* **2012**, *1* (4), 513–518.

(19) Brown, J. R.; Seo, Y.; Hall, L. M.; Lowrie, W. G. Ion Correlation Effects in Salt-Doped Block Copolymers. *Phys. Rev. Lett.* **2018**, *120*.

(20) Qin, J.; de Pablo, J. J. Ordering Transition in Salt-Doped Diblock Copolymers. *Macromolecules* **2016**, *49* (9), 3630–3638.

(21) Wang, Z. G. Effects of Ion Solvation on the Miscibility of Binary Polymer Blends. *J. Phys. Chem. B* **2008**, *112* (50), 16205–16213.

(22) Nakamura, I.; Balsara, N. P.; Wang, Z. G. Thermodynamics of Ion-Containing Polymer Blends and Block Copolymers. *Phys. Rev. Lett.* **2011**, *107* (19), 1–5.

(23) Ruzette, G.; Soo, P. P.; Sadoway, D. R.; Mayes, A. M. Melt-Formable Block Copolymer Electrolytes for Lithium Rechargeable Batteries. *J. Electrochem. Soc.* **2001**, *148* (6), A537–A543.

(24) Ren, C. L.; Nakamura, I.; Wang, Z. G. Effects of Ion-Induced Cross-Linking on the Phase Behavior in Salt-Doped Polymer Blends. *Macromolecules* **2016**, *49* (1), 425–431.

(25) Sing, C. E.; Zwanikken, J. W.; Olvera De La Cruz, M. Ion Correlation-Induced Phase Separation in Polyelectrolyte Blends. *ACS Macro Lett.* **2013**, *2* (11), 1042–1046.

(26) Sing, C. E.; Zwanikken, J. W.; de la Cruz, M. O. Electrostatic Control of Block Copolymer Morphology. *Nat. Mater.* **2014**, *13*, 694–698.

(27) Sing, C. E.; Zwanikken, J. W.; De La Cruz, M. O. Theory of Melt Polyelectrolyte Blends and Block Copolymers: Phase Behavior, Surface Tension, and Microphase Periodicity. *J. Chem. Phys.* **2015**, *142* (3).

(28) Pryamitsyn, V. A.; Kwon, H.-K.; Zwanikken, J. W.; Olvera de la Cruz, M. Anomalous Phase Behavior of Ionic Polymer Blends and Ionic Copolymers. *Macromolecules* **2017**, *50* (13), 5194–5207.

(29) Hadjichristidis, N.; Iatrou, H.; Pispas, S.; Pitsikalis, M. Anionic Polymerization: High Vacuum Techniques. *J. Polym. Sci. Part A Polym. Chem.* **2000**, *38* (18), 3211–3234.

(30) Teran, A. a.; Balsara, N. P. Thermodynamics of Block Copolymers with and without Salt. *J. Phys. Chem. B* **2014**, *118* (1), 4–17.

(31) Chintapalli, M.; Timachova, K.; Olson, K. R.; Mecham, S. J.; Devaux, D.; DeSimone, J. M.; Balsara, N. P. Relationship between Conductivity, Ion Diffusion, and Transference Number in Perfluoropolyether Electrolytes. *Macromolecules* **2016**, acs.macromol.6b00412.

(32) Thelen, J. L.; Teran, A. A.; Wang, X.; Garetz, B. A.; Nakamura, I.; Wang, Z.-G.; Balsara, N. P. Phase Behavior of a Block Copolymer/Salt Mixture through the Order-to-Disorder Transition. *Macromolecules* **2014**, *47* (8), 2666–2673.

(33) Gomez, E. D.; Panday, A.; Feng, E. H.; Chen, V.; Stone, G. M.; Minor, A. M.; Kisielowski, C.; Downing, K. H.; Borodin, O.; Smith, G. D.; et al. Effect of Ion Distribution on Conductivity of Block Copolymer Electrolytes. *Nano Lett.* **2009**, *9* (3), 1212–1216.

(34) Gilbert, J. B.; Luo, M.; Shelton, C. K.; Rubner, M. F.; Cohen, R. E.; Epps, T. H. Determination of Lithium-Ion Distributions in Nanostructured Block Polymer Electrolyte

Thin Films by X-Ray Photoelectron Spectroscopy Depth Profiling. *ACS Nano* **2015**, *9* (1), 512–520.

(35) Gartner, T. E.; Morris, M. A.; Shelton, C. K.; Dura, J. A.; Epps, T. H. Quantifying Lithium Salt and Polymer Density Distributions in Nanostructured Ion-Conducting Block Polymers. *Macromolecules* **2018**, *51* (5), 1917–1926.

(36) Loo, W. S.; Jiang, X.; Maslyn, J. A.; Oh, H. J.; Zhu, C.; Downing, K. H.; Balsara, N. P. Reentrant Phase Behavior and Coexistence in Asymmetric Block Copolymer Electrolytes. *Soft Matter* **2018**, *14* (15), 2789–2795.

(37) Hexemer, A.; Bras, W.; Glossinger, J.; Schaible, E.; Gann, E.; Kirian, R.; MacDowell, A.; Church, M.; Rude, B.; Padmore, H. A SAXS/WAXS/GISAXS Beamline with Multilayer Monochromator. In *Journal of Physics: Conference Series*; 2010; Vol. 247, p 012007.

(38) Ilavsky, J. Nika: Software for Two-Dimensional Data Reduction. *J. Appl. Crystallogr.* **2012**, *45* (2), 324–328.

(39) Wang, X.; Chintapalli, M.; Newstein, M. C.; Balsara, N. P.; Garetz, B. A. Characterization of a Block Copolymer with a Wide Distribution of Grain Sizes. *Macromolecules* **2016**, acs.macromol.6b01380.

(40) Wang, X.; Li, X.; Loo, W.; Newstein, M. C.; Balsara, N. P.; Garetz, B. A. Depolarized Scattering from Block Copolymer Grains Using Circularly Polarized Light. *Macromolecules* **2017**, *50* (13), 5122–5131.

(41) Balsara, N. P.; Perahia, D.; Safinya, C. R.; Tirrell, M. V.; Lodge, T. P. Birefringence Detection of the Order-to-Disorder Transition in Block Copolymer Liquids. *Macromolecules* **1992**, *25* (15), 3896–3901.

(42) Nakamura, I.; Balsara, N. P.; Wang, Z. G. First-Order Disordered-to-Lamellar Phase Transition in Lithium Salt-Doped Block Copolymers. *ACS Macro Lett.* **2013**, *2* (6), 478–481.

(43) Wang, X.; Thelen, J. L.; Teran, A. A.; Chintapalli, M.; Nakamura, I.; Wang, Z. G.; Newstein, M. C.; Balsara, N. P.; Garetz, B. A. Evolution of Grain Structure during Disorder-to-Order Transitions in a Block Copolymer/Salt Mixture Studied by Depolarized Light Scattering. *Macromolecules* **2014**, *47* (16), 5784–5792.

(44) Mai, S.; Fairclough, J. P. A.; Hamley, I. W.; Matsen, M. W.; Denny, R. C.; Liao, B.; Booth, C.; Ryan, A. J. Order - Disorder Transition in Poly (Oxyethylene) - Poly (Oxybutylene) Diblock Copolymers. *Macromolecules* **1996**, *29* (19), 6212–6221.

(45) Teran, A. A.; Mullin, S. A.; Hallinan, D. T.; Balsara, N. P. Discontinuous Changes in Ionic Conductivity of a Block Copolymer Electrolyte through an Order-Disorder Transition. *ACS Macro Lett.* **2012**, *1* (2), 305–309.

(46) Balsara, N. P.; Garetz, B. a.; Dai, H. J. Relationship between Birefringence and the Structure of Ordered Block Copolymer Materials. *Macromolecules* **1992**, *25* (22), 6072–6074.

(47) Grzywacz, P.; Qin, J.; Morse, D. C. Renormalization of the One-Loop Theory of Fluctuations in Polymer Blends and Diblock Copolymer Melts. *Phys. Rev. E - Stat. Nonlinear, Soft Matter Phys.* **2007**, *76* (6), 1–33.

(48) Morse, D. C.; Chung, J. K. On the Chain Length Dependence of Local Correlations in Polymer Melts and a Perturbation Theory of Symmetric Polymer Blends. *J. Chem. Phys.* **2009**, *130* (22), 224902–284902.

(49) Spencer, R. K. W.; Matsen, M. W. Critical Point of Symmetric Binary Homopolymer

Blends. *Macromolecules* **2016**, *49* (16), 6116–6125.

(50) Knychała, P.; Timachova, K.; Banaszak, M.; Balsara, N. P. 50th Anniversary Perspective: Phase Behavior of Polymer Solutions and Blends. *Macromolecules*. 2017, pp 3051–3065.

(51) Chintapalli, M.; Le, T. N. P.; Venkatesan, N. R.; Mackay, N. G.; Rojas, A. A.; Thelen, J. L.; Chen, X. C.; Devaux, D.; Balsara, N. P. Structure and Ionic Conductivity of Polystyrene-Block -Poly(Ethylene Oxide) Electrolytes in the High Salt Concentration Limit. *Macromolecules* **2016**, *49* (5), 1770–1780.

(52) Shultz, A. R.; Flory, P. J. Phase Equilibria in Polymer-Solvent Systems1,2. *J. Am. Chem. Soc.* **1952**, *74*, 4760−4767.

(53) Bae, Y. C.; Shim, J. J.; Soane, D. S.; Prausnitz, J. M. Representation of Vapor–liquid and Liquid–liquid Equilibria for Binary Systems Containing Polymers: Applicability of an Extended Flory–huggins Equation. *J. Appl. Polym. Sci.* **1993**, *47* (7), 1193–1206.

(54) Khandpur, A. K.; Förster, S.; Bates, F. S.; Hamley, I. W.; Ryan, A. J.; Bras, W.; Almdal, K.; Mortensen, K. Polyisoprene-Polystyrene Diblock Copolymer Phase Diagram near the Order-Disorder Transition. *Macromolecules* **1995**, *28* (26), 8796–8806.

TOC Graphic

Phase Behavior of Mixtures of Block Copolymers and a Lithium Salt